Partial Differential Equations in Applied Mathematics 10 (2024) 100666

Contents lists available at ScienceDirect

Partial Differential Equations in Applied Mathematics

journal homepage: www.elsevier.com/locate/padiff

Unsteady magnetohydrodynamic squeezing Darcy-Forchheimer flow of Fe_3O_4 Casson nanofluid: Impact of heat source/sink and thermal radiation

Shimaa E. Waheed [a,*], Galal M. Moatimid [b], Abeer S. Elfeshawey [a]

[a] Department of Mathematics, Faculty of Science, Benha University, Benha 13518, Egypt
[b] Department of Mathematics, Faculty of Education, Ain Shams University, Cairo, Egypt

ARTICLE INFO

Keywords:
Squeezing stream
Casson nanofluid
Slip condition
Magnetohydrodynamics
Melting effect
Porous medium
Heat source
Thermal radiation
Homotopy perturbation method

ABSTRACT

The paper aims to investigate the unsteady magnetohydrodynamics (MHD) flow with Darcy-Forchheimer effect and heat transportation. The system incorporates a Casson nanofluid (CNF) with heat transfer during melting and slip velocity, influenced by heat source/sink and thermal radiation. The motivation of investigating the current topic comes because of the squeeze flow is of practical physics. The mathematical process involves converting nonlinear partial differential equations (PDEs) into nonlinear ordinary differential equations (ODEs). The nonlinear ODEs are analytically solved via the Homotopy perturbation method (HPM), while considering the appropriate boundary conditions (BCs). Through a non-dimensional procedure, many dimensionless physical quantities are achieved. The primary results of velocity, temperature profiles, local skin-friction, and the local Nusselt number are shown and analyzed based on several non-dimensional parameters. It is found that the increasing of the radiation factor values, leads to a drop in the velocity and temperature of the CNF, as well as the local skin-friction and Nusselt number. Additionally, the increase of the slip velocity factor results in higher velocity, temperature, and local Nusselt number. Meanwhile, it reduces the local skin-friction.

1. Introduction

Squeeze flow was a kind of flow that finds its uses in the processing of materials, lubrication, and rheology. It occurred when a fluid was compressed between two opposite plates that were nearing one another and was subsequently squeezed out radially. Investigations were conducted on the effects of temperature, velocity, and varied fluid characteristics on the time-dependent MHD squeezing flow of nanofluids between two parallel discs with transpiration.[1] It was discovered that the flow field was significantly impacted by the temperature-dependent thermophysical characteristics. Investigators looked into an analytical solution of the slow squeeze flow of a slightly viscoelastic fluid film between two circular discs, where the lower disc was kept stationary and the upper disc approached it at a constant speed.[2] The goal of the study was to use the Langlois recursive approach to determine how the differential type fluid behaved on a steady squeezing flow. The impact of the temperature-dependent binary chemical reaction on the flow of hydromagnetic viscous fluid through a porous material as a result of the squeezing phenomenon was examined theoretically.[3] Arrhenius activation energy was also considered to improve comprehension of changes in the processes of convective heat and mass transport (MHT). Under the influence of a uniform transverse MF, the velocity profile of an incompressible viscous fluid being squeezing through a porous media was investigated.[4] With the use of vortices and stream functions, the continuity and momentum equations were simultaneously converted to ODEs. The effects of chemical reaction on MHD squeezing flow of CNF across a permeable media in the slip condition with viscous dissipation were investigated and driven by the application of the flow in the industry difficulties.[5] Additionally, it was shown that the mass transfer rate was increased in destructive chemical reactions, while negative outcomes were observed in constructive chemical reactions. A novel iterative method was used to analyze the steady two-dimensional axisymmetric flow of an incompressible viscous fluid with slip BC in a porous media under the influence of a uniform transverse MF.[6] A novel class of fluids known as stress power-law fluids, described by an implicit relation, was studied in terms of the squeezing flow between circular discs.[7] A theoretical examination was reported on the effects of changing mass diffusivity, thermal conductivity, and viscosity on the unsteady squeezed flow of dissipative CNF.[8] Physically, to achieve the intended manufacturing output, an accurate accounting of the thermophysical parameters of such a system was necessary for any efficient MHT process. Using the differential transform approach, the effects of thermal radiation and MF on the squeezing flow and heat transfer of third-grade

* Corresponding author.
E-mail address: shaimaa.riyadh@fsc.bu.edu.eg (S.E. Waheed).

https://doi.org/10.1016/j.padiff.2024.100666
Received 17 February 2024; Received in revised form 18 March 2024; Accepted 20 March 2024
Available online 5 April 2024

Nomenclature

a	slip factor
$B(t)$	magnetic field (MF) (Am^{-1}) ampere per meter
B_0	imposed MF (Wbm^{-2})
c_b	coefficient of porous medium (m^2)
Cf_x	local skin-friction coefficient
c_p	specific heat at constant pressure ($kg^{-1}K^{-1}J$)
c_s	heat capacity of the solid surface
E_c	local Eckert numeral
e_{ij}	rate of strain (deformation)
f	non-dimensional stream function
F_r	Forchheimer factor
$h(t)$	gap width between the two plates (m)
K_1	permeability of the porous medium (m^2)
K	porous factor
k^*	mean absorption coefficient
l	distant-apart between the two sheets
M	magnetic factor
M_e	melting factor
Nu_x	local Nusselt numeral
Pr	Prandtl numeral
q_r	radiative heat flux
$Q(t)$	heat source
R_d	radiation factor (Wm^2K^{-1})
Re_x	local Reynolds numeral
S	squeeze factor
T	temperature of fluid (K)
T_m	melting surface temperature (K)
T_w	upper surface temperature (K)
T_0	solid temperature (K)
u_w	velocity of sheet (m/s)
u, v	fluid velocity component along x, y axes (m/s)
x, y	Cartesian coordinates (m)

Greek symbols

τ_{ij}	shear stress(Pa)
π	component of deformation rate product
β	Casson factor
μ_B	plastic dynamic viscosity
κ	thermal conductivity coefficient ($Wm^{-1}K^{-1}$)
γ_0	slip velocity factor
γ	heat generation/absorption factors
μ_B	dynamic fluid viscosity (Pas)
μ	dynamic viscosity ($kgm^{-1}s^{-1}$)
η	similarity variable
λ	latent heat fluid
α	non-dimensional constant
ϕ	non-dimensional nanoparticle volume fraction ($molm^{-3}$)
θ	non-dimensional temperature
σ	electric conductivity (Sm^{-1})
σ_1	Stefan–Boltzmann constant
ρ	fluid density (kgm^{-3})

Superscripts

$'$	variation concerning η

Subscripts

nf	nano-fluid
p	nano particle
w	wall condition

nanofluid between two discs imbedded in a porous media with temperature jump BCs were examined.[9] Under the effect of innovative changing diffusivity, the heat and mass transfer in an unstable squeezing flow between parallel plates was investigated.[10] The majority of the literature, held the opinion that the fluid's thermophysical characteristics remained constant.

Throughout the last decades, the significance of nanoparticles has changed because of their vital roles in many thermo physical processes and their enhanced environmental evident. Similar to nanofluids, the hybrid fluids preserved outstanding energy transportation. Similar materials were used in evident domains, such as military hardware and solar collectors. An analysis was conducted on the significant impact of thermal radiation on Joule heating caused by wall jet blood flow, when a hybrid nanofluid was present over the moving surface.[11] Utilizing the influence of the convective heating boundary and Lorentz force on second-grade nanofluid flow in conjunction with a Riga pattern was demonstrated.[12] The Grinberg term and a Lorentz force applied parallel to the Riga plate wall were used to create the model. The characteristics of MHT events in the two-dimensional viscous liquid flow of Oldroyd-B nanofluid were theoretically examined.[13] By considering the effects of mixed convection and inclined MFs, the fluid was over a vertically stretched sheet that included gyrotactic microorganisms. Through heat generation or absorption, a two-dimensional MHD flow and MHT phenomena of a water-based nanofluid containing gyrotactic microorganisms over a vertical plate were analyzed.[14] A vertically stretched sheet containing swimming gyrotactic microorganisms was subjected to a viscoelastic Oldroyd-B nanofluid flow study.[15] The Lorentz force characteristics were reflected due to the normal application of the MF on the sheet. In a nano liquid-saturated porous media, the Darcy free convection around an isothermal vertical cone with a fixed apex half-angle pointing downward was investigated.[16] It was supposed that the medium was made up of nanoparticle-containing oxytactic bacteria. Two hybrid nanofluids and a well-known nanofluid flow over a stretchable spinning cylinder were shown to have the same hydrothermal feature.[17] The impacted flow appropriated grapheme and ferrous nanoparticles from the current fluids. It was investigated what made the mass and thermal convective boundary limitations appealing.[18] A rotating stretchable disc-induced free convective flow of non-Newtonian nanofluid was examined.[19] As an accurate illustrative model, the analysis covers the Stefan blowing and CattaneoChristov mass and heat fluxes. The study's novel parts were the use of thermophoresis to analyze boundary sheet nanofluid flow close to a rotating disc, the study of random nanoparticle motion, and the investigation of Reiner-Rivlin prototype characteristics.

There are numerous engineering applications for CNF research. In a three-dimensional mixing biological convection flow of CNF inside a stretching cylinder, the properties of heat production and absorption were investigated.[20] Notably, greater viscosity and flow resistance were linked to higher Casson parameter values. By submerging ternary hybrid nanoparticles, a study was conducted to improve and evaluate the thermal performance of non-Newtonian Casson fluid $Fe_3O_4 - Al_2O_3 - TiO_2$.[21] A system of complex transport differential equations was created by applying a non-Fourier heat transfer model of the transportation of energy to theoretically simulate the behavior of such complex events. By using a tri-hybrid Yamada-Ota and Xue nanofluid model, the impact of diathermic oil by the addition of tri-hybrid nanoparticles was created.[22] The work was unique in that it examined a previously unexplored aspect of tri-hybrid nanoparticles: the extension of the Yamada-Ota and Xue nanofluid models in the body's existing literature. It was proposed to use a three-dimensional CNF based on applied magnetics features and a new nonlinear thermal radiation.[23] The thermophoretic and Brownian mechanisms were explained using the modified Buongiorno thermal

nano model. A unique porous cone-bounded mathematical ternary hybrid nanofluid flow model was created.[24] Better heat transfer outcomes through thermal radiation and viscous dissipation were the goals of the investigation. An analysis was done on the validity of thermal radiation on the time-dependent stream of the CF caused by an inclined surface that accelerated exponentially in addition to thermal and solutal convective BCs.[25] Additionally, the analysis was done on the MHD of the CNF stream through porous media.[26] The CNF problem over a nonlinear stretched sheet with MHT and stagnation point stream was examined.[27] Furthermore, velocity slip was used to investigate the second law of MHD of the CNF over an expanding sheet.[28,29] Their results showed that heat transmission was accelerated by the Casson factor. A multilayer stretched cylinder containing gyrotactic microorganisms was exposed to a magnetized and non-magnetized CNF stream.[30]

Most structures in the universe were nonlinear in their nature. Finding solutions to nonlinear problems interested a broad spectrum of scientists, including mathematics, biologists, engineers, and many others. Therefore, it was unlikely that the majority of differential equations would have analytical solutions. Additionally, numerical methods were commonly used. Moreover, it was common for multiple nonlinear equations to lack a small factor at the same time, and the conventional perturbation method relies on this small value. The application of conventional methods was affected by this restriction. The small factor determination was a challenging process that required the use of sophisticated methods. The HPM was one of the modern perturbation techniques. It was employed in the establishment of semi-analytical or approximate analytical solutions for differential equations belonging to several classes. It combined the advantages of the Homotopy analysis and the classic perturbation methods into a single method. It was thought that Professor He, as a Chinese Mathematician, was the first investigator who introduced this novel approach.[31] As a result, this technique involved an inserting little factor known as the Homotopy artificial factor$q \in [0, 1]$. The given problem was divided into linear and nonlinear components by this factor q. As,$q = 0$, there exists an exact solution to the differential equation known as the Homotopy equation. As is widely known, the produced approximation was consistently valid for extremely high values and small factor values. There were several uses for the HPM in nonlinear PDEs as well as nonlinear ODEs. The zero and higher-order solutions to the Homotopy equation, which fluctuates between zero and unity, were included. In this way, the ideal solution looked like the required form. The actual equilibrium point criteria were investigated in the context of HPM.[32] Burger's problem was addressed using the variational iteration approach and HPM for the analysis of water satisfied in an unsaturated permeable medium.[33] The impact of spacing gaps and the electrical characteristics of the streaming Rabinowitsch stream were analyzed using the HPM.[34] The nonlinear Electrohydrodynamics (EHD) instability of a cylinder-shaped interface between two viscoelastic fluids of Walters' B type, in a porous medium, was studied.[35] Many special situations with appropriate data selections were given. Laplace transformations and a modified version of the HPM were used.[36,37] To produce a uniform valid expansion of various nonlinear ODEs, the concept of expanded nonlinear frequency was also utilized. The motile microorganisms through an MHD stream of an incompressible nanofluid obeying the non-Newtonian Jeffrey prototype were investigated.[38] An important benefit of this approach was that it can solve a large number of nonlinear problems in applied sciences, without the requirement for a small factor in the equation. Therefore, the present work depends mainly on this approach.

In light of the aforementioned aspects, the purpose of this research is to study an analytical solution for squeezing motion of the Fe_3O_4 CNF of Darcy-Forchheimer stream. The motion is considered in the existence of radiation and under the influence of the MF, heat generation/absorption, slip velocity, and melting heat transport. In principle, we wish to extend for Fe_3O_4 CNF the previous problem,[39] which neglected many important physical parameters such as activation generation/absorption, melting heat transport, and slip velocity parameter. The squeezing stream of the CNF is reflected because of its uses in a range of technical applications, including medical purposes. The great importance of slip velocity in energy-related applications, such as solar collectors and thermal energy storage systems, are also included.[40] The present study provides a significant contribution in high-temperature and cooling processes, conductive coating, paints, space technology medicines, and bio-sensors.

At the end of this study, the following questions are expected to be answered:

- How do the velocity components behave for a squeezing stream of a non-Newtonian CNF under the effect of various factors?
- What is the behavior of the temperature distributed through this stream?
- What are the impacts of the various factors on the most popular physical quantities of local skin fraction and local Nusselt numerals?

To clarify the presentation of the paper, the subsequent sections are arranged as follows: The formulation of the problem is elucidated in **§ 2**, where the main equations of motion along with appropriate BCs are outlined. In **§ 3**, an illustration to produce an analytic solution using HPM is provided. The results and arguments are positioned in **§ 4**. Finally, the principal findings are outlined in **§ 5**.

2. Formulation of problem

An unsteady two-dimensional incompressible squeezed Darcy-Forchheimer movement of Fe_3O_4 CF with melting heat transport and slip velocity effect is considered with the metricy $= \pm h(t) = \pm l\sqrt{(1-\alpha t)}$, where l is the initial distance between two plates. For$1/t > \alpha > 0$, the two plates are compressed until they come into contact with each other$t = 1/\alpha$, while $\alpha < 0$the two plates move at a distance apart. Considering the Cartesian coordinate system, the lowest plate is positioned at $y = 0$, meanwhile the upper is a located ath(t) as displayed in Fig. 1.

A non-uniform MF $B(t) = B_0(1 - \alpha t)^{-1/2}$ of constant strength B_0 is affected along with the positive $y -$ path normal to the stream path. Additionally, it is also presumed that the velocity of the upper flow is given as$u_w(x) = \frac{\alpha x}{2(1-\alpha t)}$. The parameter T_m is the melting surface temperature; simultaneously the temperature in the upper plate form is given byT_w, where $T_w > T_m$. The rheologic equation of municipal for an isotropic flow of the CNF is given as[41]:

$$\tau_{ij} = \begin{cases} 2\left(\mu_B + \dfrac{P_y}{\sqrt{2\Omega}}\right)e_{ij}, & \Omega > \Omega_c \\ 2\left(\mu_B + \dfrac{P_y}{\sqrt{2\Omega}}\right)e_{ij}, & \Omega < \Omega_c \end{cases}, \tag{1}$$

where $\Omega = e_{ij}e_{ij}$ is the ijelement of distortion rate, Ω denotes the production of the element of distortion rate with itself, $\Omega_c$shows that the non-Newtonian model which determines a crucial threshold for this product, $P_y = \mu_B\sqrt{2\Omega_c}/\beta$ is the generated stress of fluid, and β is the Casson factor.

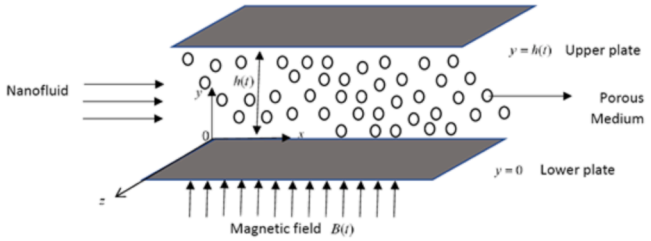

Fig. 1. Sketch of theoretical model.

Considering the aforementioned factors, the main equations for the boundary layer that describe the transport of stream and heat are[39,41,42] as follows:

$$\frac{\partial u}{\partial x}+\frac{\partial v}{\partial y}=0, \tag{2}$$

$$\frac{\partial u}{\partial t}+u\frac{\partial u}{\partial x}+v\frac{\partial u}{\partial y}=\frac{-1}{\rho_{nf}}\frac{\partial P}{\partial x}+\frac{\mu_{nf}}{\rho_{nf}}\left(1+\frac{1}{\beta}\right)\left(\frac{\partial^2 u}{\partial x^2}+\frac{\partial^2 u}{\partial y^2}\right) - \frac{1}{\rho_{nf}}\left(\sigma B^2(t)+\frac{\mu_{nf}}{K_1}\right)u-\frac{c_b}{\sqrt{K_1}}u^2, \tag{3}$$

$$\frac{\partial v}{\partial t}+u\frac{\partial v}{\partial x}+v\frac{\partial v}{\partial y}=\frac{-1}{\rho_{nf}}\frac{\partial P}{\partial y}+\frac{\mu_{nf}}{\rho_{nf}}\left(1+\frac{1}{\beta}\right)\left(\frac{\partial^2 v}{\partial x^2}+\frac{\partial^2 v}{\partial y^2}\right)-\left(\frac{\mu_{nf}}{\rho_{nf}K_1}\right)v-\frac{c_b}{\sqrt{K_1}}v^2, \tag{4}$$

and

$$\frac{\partial T}{\partial t}+u\frac{\partial T}{\partial x}+v\frac{\partial T}{\partial y}=\frac{\kappa_{nf}}{(\rho c_p)_{nf}}\left(\frac{\partial^2 T}{\partial x^2}+\frac{\partial^2 T}{\partial y^2}\right)-\frac{1}{(\rho c_p)_{nf}}\frac{\partial q_r}{\partial y}+\frac{Q(t)(T-T_w)}{(\rho c_p)_{nf}}. \tag{5}$$

where $Q(t)=Q_0/(1-\alpha t)$ is the heat source.

The above equations are solved dependent along with the following BCs[41]:

$$\left.\begin{aligned} y=0 \;\Rightarrow u=u_w+\gamma_0\left(1+\frac{1}{\beta}\right)\frac{\partial u}{\partial y}, \quad T=T_0\\ y=h(t) \;\Rightarrow\; u=0 \;\&\; v=\frac{dh}{dt} \quad \&\quad T=T_w \end{aligned}\right\}, \tag{6}$$

and

$$\kappa_{nf}\left(\frac{\partial T}{\partial y}\right)\Big|_{y=0}=\rho_{nf}[\lambda+c_s(T_m-T_0)]v_0, \tag{7}$$

Eq. (7) shows that the amount of heat conducted to the surface undergoing melting is equal to the heat of fusion, as well as the sensible heat needed to raise the temperature of the solid T_0 to its melting temperature T_m[43]:

The different thermophysical properties of the nanofluid have mathematical expressions as[44]:

$$\mu_{nf}=\frac{\mu_f}{(1-\phi)^{2.5}},\ \text{(Brinkman)} \tag{8}$$

$$\rho_{nf}=(1-\phi)\rho_f+\phi\rho_p, \tag{9}$$

$$(c_p)_{nf}=(1-\phi)(c_p)_f+\phi(c_p)_p, \tag{10}$$

$$\frac{\kappa_{nf}}{\kappa_f}=\frac{(\kappa_p+2\kappa_f)-2\phi(\kappa_f-\kappa_p)}{(\kappa_p+2\kappa_f)+2\phi(\kappa_f-\kappa_p)}.\ \text{(Maxwell}-\text{Garnett)} \tag{11}$$

The radiative heat flux q_r is determined using the Rosseland approximation in such a way that[45]:

$$q_r=-\frac{4\sigma_1}{3k^*}\frac{\partial T^4}{\partial y}. \tag{12}$$

We can extend T^4 about T_m in the Taylor's series and drop out the higher orders, and then we get:

$$T^4=4T_m^3T-3T_m^4. \tag{13}$$

For a similarity solution, the following non-dimensional variables are introduced[39]:

$$\left.\begin{aligned} \eta=\frac{y}{l\sqrt{1-\alpha t}} \;\&\; \theta=\frac{T-T_m}{T_w-T_m}\\ u=\frac{\alpha x}{2(1-\alpha t)}f'(\eta) \;\&\; v=\frac{-\alpha l}{2\sqrt{1-\alpha t}}f(\eta) \end{aligned}\right\}, \tag{14}$$

where f, and θ are the non-dimensional velocity and temperature distributions, respectively.

Using the variables given in Eq. (14) and Eqs. (7)–(12), Eqs. (2)–(6) are transformed to the following nonlinear ODE:

$$\left(\frac{1}{1+\beta}\right)f^{iv}-S\frac{A_3}{A_2}(\eta f'''-ff''+f'f''+3f'')-\left(K+\frac{M}{A_2}\right)f''-F_r\frac{A_3}{A_2}f'f''=0, \tag{15}$$

$$\left(A_1+\frac{4}{3}R_d\right)\theta''+S\mathrm{Pr}A_4\theta'(f-\eta)+\gamma\theta=0. \tag{16}$$

with the applicable BCs:

$$\eta=0:\ f'=1+a\left(1+\frac{1}{\beta}\right)f'',\ M_e\theta'+S\mathrm{Pr}\frac{A_3}{A_1}f=0,\ \theta=0, \tag{17}$$

$$\eta=1:\ f'=0,\ f=1,\ \theta=1. \tag{18}$$

where

$$\left.\begin{aligned} A_1=\frac{\kappa_{nf}}{\kappa_f}=\frac{(\kappa_p+2\kappa_f)-2\phi(\kappa_f-\kappa_p)}{(\kappa_p+2\kappa_f)+2\phi(\kappa_f-\kappa_p)}\&A_2=\frac{\mu_{nf}}{\mu_f}=(1-\phi)^{-2.5}\\ A_3=\frac{\rho_{nf}}{\rho_f}=(1-\phi)+\phi\frac{\rho_p}{\rho_f}\ \&A_4=\frac{(\rho c_p)_{nf}}{(\rho c_p)_f}=(1-\phi)+\phi\frac{(\rho c_p)_p}{(\rho c_p)_f} \end{aligned}\right\}. \tag{19}$$

The factors used in the system of the ODEs are given in Eqs. (15)–(17), where $S=\alpha l^2/2\nu_f$ is the squeeze factor, $K=(1-\alpha t)l^2/K_1$ is the porous factor, $F_r=\alpha l^2c_bx/\sqrt{K_1}$ is the Forchheimer factor, $M=\sigma B_0^2l^2/\mu_f$ is the magnetic factor, $a=\gamma_0/l\sqrt{1-\alpha t}$ is the slip factor, $R_d=4\sigma_1{T_m}^3/\kappa^*\kappa_f$ is the radiation factor, $\gamma=Q_0l^2/\kappa_f$ is the heat generation/absorption factors, $\mathrm{Pr}=\mu_f(c_p)_f/\kappa_f$ is the Prandtl numeral, and $M_e=(c_p)_f(T_w-T_m)/[\lambda+c_s(T_m-T_0)]$ is the melting factor.

The physical quantities of interest in this problem are the local skin friction coefficient Cf_x and the local Nusselt numeral Nu_x which can be expressed as:

$$Cf_x\sqrt{(1-\alpha t)}\mathrm{Re}_x\Big/2=\frac{A_2}{A_3}\left(1+\frac{1}{\beta}\right)f'(0), \tag{20}$$

and

$$Nu_x\sqrt{(1-\alpha t)}=-A_1\theta'(0). \tag{21}$$

where $\mathrm{Re}_x=u_wl/\upsilon$ is the local Reynolds number.

3. Methodology

As well known, all perturbation methods aim to convert the nonlinear ODEs into a system of linear ones. It is said that the HPM is a relatively recently developed analytical method for finding approximation solution to the given equation. It does away with the limitations of traditional perturbation methods, while combining their benefits.

The innovation of the method is solving some linear and nonlinear ODEs in both analytically and approximately. It appears from the previous data that the governing system of nonlinear ODEs may be analyzed using the HPM method. As previously shown, the similarity transform yields the ODEs as given in Eqs. (15), and (16), and they are subjected to the BCs as provided in Eqs. (17), and (18). In light of the framework of the HPM, any differential equation can be divided into linear and nonlinear parts as shown in the introductory section.

A synthetic factor is provided to create this distinction and can be identified by the parameter q. This factor is used to create the well-known Homotopy equation, which effectively divides the governing equations into linear and nonlinear portions. As a result, the previously given equations can be written as follows: the linear part indicates the linear operator, meanwhile the nonlinear part $L[u]=0$, where L denotes the linear operator. Temporarily, the nonlinear part $N[u]=0$, where

Nrefers to the nonlinear operator. The non-linear parts of the influence of the fundamental equations are managed by the synthetic factor$q$. Actually, the linear part of the Homotopy equation has an exact solution. After the substitution from the zero-order into the higher-orders, one gets another system on nonhomogeneous linear differential equations. Therefore, it is possible to approximate the solution to the original nonlinear ODEs by solving the resulting linear equations.

$$h(f,q) = L_1(f) + q\left[-S\frac{A_3}{A_2}(\eta f''' - f f'' + f' f'' + 3f'') - \left(K + \frac{M}{A_2}\right) f'' - F_r \frac{A_3}{A_2} f' f'' \right] = 0 \tag{22}$$

and $$h(\theta,q) = L_2(\theta) + q[S\mathrm{Pr}A_4\theta'(f-\eta) + \gamma\theta] = 0, \tag{23}$$

where, $L_1(f) = \left(1+\frac{1}{\beta}\right) f^{iv}$ and $L_2(\theta) = \left(A_1 + \frac{4}{3}R_d\right)\theta''$ are linear operators. where $q \in [0, 1]$ is a nearby factor used to expand the solution in the following forms:

$$\left.\begin{array}{l} f(\eta,q) = f_0 + qf_1 + q^2 f_2 + \ldots\ldots\ldots\ldots \\ \theta(\eta,q) = \theta_0 + q\theta_1 + q^2\theta_2 + \ldots\ldots\ldots\ldots \end{array}\right\}. \tag{24}$$

Substituting from Eq. (24) into Eqs. (22) and (23), by equating terms with the same powers of q, we can find a system of $n+1$linear ODEs. Suppose$n = 1$, the system is as follows:

- **Zero-order system**:

$$\left(1+\frac{1}{\beta}\right) f_0^{iv} = 0, \tag{25}$$

and $$\left(A_1 + \frac{4}{3}R_d\right)\theta''_0 = 0. \tag{26}$$

Along with the appropriate BCs, one gets

$$\left.\begin{array}{c} f'_0(0) = 1 + a\left(1+\frac{1}{\beta}\right) f''_0(0) \;\&M_e\theta'_0(0) + S\mathrm{Pr}\frac{A_3}{A_1} f_0(0) = 0,\ \&f_0(1) = 1,\ \& f'_0(1) = 0 \\ \theta_0(0) = 0 \;\&\; \theta_0(1) = 1 \end{array}\right\}. \tag{27}$$

- **First-order system**:

$$\left(1+\frac{1}{\beta}\right) f_1^{iv} = S\frac{A_3}{A_2}[\eta f'''_0 - f_0 f''_0 + f'_0 f''_0 + 3f''_0] + \left(K + \frac{M}{A_2}\right) f''_0 + F_r\frac{A_3}{A_2} f'_0 f''_0], \tag{28}$$

and

$$\left(A_1 + \frac{4}{3}R_d\right)\theta''_1 = -S\mathrm{Pr}A_4\theta'_0(f_0 - \eta) - \gamma\theta_0. \tag{29}$$

With the suitable BCs:

$$\left.\begin{array}{c} f'_1(0) = a\left(1+\frac{1}{\beta}\right) f''_1(0),\ \ M_e\theta'_1(0) + S\mathrm{Pr}\frac{A_3}{A_1} f_1(0) = 0,\ \ f_1(1) = 0,\ \ f'_1(1) = 0 \\ \theta_1(0) = 0 \;\&\; \theta_1(1) = 0. \end{array}\right\} \tag{30}$$

The approximate solution of the system is given in Eqs. (28)–(30) can be listed as follows:

$$f_0 = \frac{\alpha_1}{6}\eta^3 + \frac{\alpha_2}{2}\eta^2 + \alpha_3\eta + \alpha_4, \tag{31}$$

$$\theta_0 = \eta, \tag{32}$$

$$f_1 = -\frac{\lambda_1\alpha_1}{10080}\eta^8 + \left[(\lambda_1+\lambda_3)\frac{{\alpha_1}^2}{2} - \frac{4\alpha_1\alpha_2\lambda_1}{6}\right]\frac{\eta^7}{840} + \left[(\lambda_1+\lambda_3)\frac{3\alpha_1\alpha_2}{2} - \left(\frac{{\alpha_2}^2}{2} + \alpha_1\alpha_3\right)\lambda_1\right]\frac{\eta^6}{360} + \left[(\lambda_1+\lambda_2)\alpha_1 + \left({\alpha_2}^2 + \alpha_1\alpha_3\right)(\lambda_1+\lambda_3) - \lambda_1(\alpha_1\alpha_4 + \alpha_2\alpha_3)\right]\frac{\eta^5}{120} + [\lambda_2\alpha_2 + \alpha_2\alpha_3(\lambda_1+\lambda_3) - \lambda_1\alpha_2\alpha_4]\frac{\eta^4}{24} + \frac{c_1}{6}\eta^3 + \frac{c_2}{2}\eta^2 + c_3\eta + c_4, \tag{33}$$

$$\theta_1 = \frac{SA_4\mathrm{Pr}}{\lambda_6}\left[-\frac{\alpha_1}{120}\eta^5 - \frac{\alpha_2}{24}\eta^4 + \left(1 - \alpha_3 - \frac{\gamma}{SA_4\mathrm{Pr}}\right)\frac{\eta^3}{6} - 4\frac{\eta^2}{2}\right] + c_5\eta, \tag{34}$$

where the constants $\lambda_1,\lambda_2,\lambda_3,\lambda_4,\lambda_5,\lambda_6,\alpha_1,\alpha_2,\alpha_3,\alpha_4,c_1,c_2,c_3,c_4,c_5$are defined as:

$$\left.\begin{array}{c} \lambda_1 = S\frac{A_3}{A_2\left(1+\beta^{-1}\right)},\quad \lambda_2 = \frac{1}{\left(1+\beta^{-1}\right)}\left(S\frac{A_3}{A_2} + \frac{M}{A_2} + K\right),\quad \lambda_3 = \frac{A_3}{A_2\left(1+\beta^{-1}\right)}F_r \\ \lambda_4 = a\left(1+\beta^{-1}\right),\quad \lambda_5 = S\mathrm{Pr}\frac{A_3}{A_1},\quad \lambda_6 = \frac{\kappa_{nf}}{\kappa_f} + \frac{4}{3}R_d, \end{array}\right\} \tag{35}$$

$$\left.\begin{array}{c} \alpha_1 = -2 - \frac{2(1+\lambda_4)}{(1/2+2\lambda_4)}\left(\frac{3M_e}{\lambda_5}+1\right),\quad \alpha_2 = \frac{1}{(1/2+2\lambda_4)}\left(\frac{3M_e}{\lambda_5}+1\right), \\ \alpha_3 = 1 + \frac{\lambda_4}{(1/2+2\lambda_4)}\left(\frac{3M_e}{\lambda_5}+1\right),\quad \alpha_4 = -\frac{M_e}{\lambda_5}, \end{array}\right\} \tag{36}$$

$$\left.\begin{aligned} c_1 &= \frac{6\Gamma_1(1+2\lambda_4)-12\Gamma_2(1+\lambda_4)}{(1+4\lambda_4)}, \quad c_2 = \frac{6\Gamma_1-2\Gamma_2}{1+4\lambda_4}, \quad c_3 = \lambda_4 c_2, \\ c_4 &= -\frac{M_e}{\lambda_5}c_5, \quad c_5 = \frac{SA_4\mathrm{Pr}}{\lambda_6}\left(\frac{\alpha_1}{120}+\frac{\alpha_2}{24}+\frac{\alpha_3}{6}+\frac{\gamma}{6SA_4\mathrm{Pr}}+\frac{\alpha_4}{2}-\frac{1}{6}\right), \end{aligned}\right\} \tag{37}$$

where

$$\left.\begin{aligned} \Gamma_1 &= \frac{\lambda_1{\alpha_1}^2}{1260}-\frac{1}{120}\left[(\lambda_1+\lambda_3)\frac{{\alpha_1}^2}{2}-\frac{4\alpha_1\alpha_2\lambda_1}{6}\right]-\frac{1}{60}\left[(\lambda_1+\lambda_3)\frac{3\alpha_1\alpha_2}{2}-\left(\frac{{\alpha_2}^2}{2}+\alpha_1\alpha_3\right)\lambda_1\right] \\ &-\frac{1}{24}\left[(\lambda_1+\lambda_2)\alpha_1+\left({\alpha_2}^2+\alpha_1\alpha_3\right)(\lambda_1+\lambda_3)-\lambda_1(\alpha_1\alpha_4+\alpha_2\alpha_3)\right]-\frac{1}{6}[\lambda_2\alpha_2+\alpha_2\alpha_3(\lambda_1+\lambda_3)-\lambda_1\alpha_2\alpha_4] \\ \Gamma_2 &= \frac{M_e}{\lambda_5}\left(\frac{SA_4\mathrm{Pr}}{\lambda_6}\right)\left(\frac{\alpha_1}{120}+\frac{\alpha_2}{24}+\frac{\alpha_3}{6}+\frac{\gamma}{6SA_4\mathrm{Pr}}+\frac{\alpha_4}{2}-\frac{1}{6}\right)+\frac{\lambda_1{\alpha_1}^2}{10080}-\frac{1}{840}\left[(\lambda_1+\lambda_3)\frac{{\alpha_1}^2}{2}-\frac{4\alpha_1\alpha_2\lambda_1}{6}\right] \\ &-\frac{1}{360}\left[(\lambda_1+\lambda_3)\frac{3\alpha_1\alpha_2}{2}-\left(\frac{{\alpha_2}^2}{2}+\alpha_1\alpha_3\right)\lambda_1\right]-\frac{1}{120}\left[(\lambda_1+\lambda_2)\alpha_1+\left({\alpha_2}^2+\alpha_1\alpha_3\right)(\lambda_1+\lambda_3)-\lambda_1(\alpha_1\alpha_4+\alpha_2\alpha_3)\right] \\ &-\frac{1}{24}[\lambda_2\alpha_2+\alpha_2\alpha_3(\lambda_1+\lambda_3)-\lambda_1\alpha_2\alpha_4], \end{aligned}\right\} \tag{38}$$

Using the identical method, we can derive the remaining elements of the solutions $f(\eta)$and$\theta(\eta)$. Therefore, the expressions presented below represent the rough estimations for the non-dimensional velocity and temperature components:

$$\left.\begin{aligned} f(\eta) &= \lim_{q\to 1}\left(f_0+qf_1+q^2f_2+\ldots\ldots\ldots\ldots\right) \\ \theta(\eta) &= \lim_{q\to 1}\left(\theta_0+q\theta_1+q^2\theta_2+\ldots\ldots\ldots\ldots\right) \end{aligned}\right\}. \tag{39}$$

Finally, the distributions of the functions $f(\eta)$and$\theta(\eta)$ can be itemized as:

$$\begin{aligned} f(\eta) &= -\frac{\lambda_1\alpha_1}{10080}\eta^8+\left[(\lambda_1+\lambda_3)\frac{{\alpha_1}^2}{2}-\frac{4\alpha_1\alpha_2\lambda_1}{6}\right]\frac{\eta^7}{840}+\left[(\lambda_1+\lambda_3)\frac{3\alpha_1\alpha_2}{2}-\left(\frac{{\alpha_2}^2}{2}+\alpha_1\alpha_3\right)\lambda_1\right]\frac{\eta^6}{360} \\ &+\left[(\lambda_1+\lambda_2)\alpha_1+\left({\alpha_2}^2+\alpha_1\alpha_3\right)(\lambda_1+\lambda_3)-\lambda_1(\alpha_1\alpha_4+\alpha_2\alpha_3)\right]\frac{\eta^5}{120}+[\lambda_2\alpha_2+\alpha_2\alpha_3(\lambda_1+\lambda_3)-\lambda_1\alpha_2\alpha_4]\frac{\eta^4}{24} \\ &\frac{(c_1+\alpha_1)}{6}\eta^3+\frac{(c_2+\alpha_2)}{2}\eta^2+(c_3+\alpha_3)\eta+(c_4+\alpha_4), \end{aligned} \tag{40}$$

$$\theta(\eta) = \frac{SA_4\mathrm{Pr}}{\lambda_6}\left[-\frac{\alpha_1}{120}\eta^5-\frac{\alpha_2}{24}\eta^4+\left(1-\alpha_3-\frac{\gamma}{SA_4\mathrm{Pr}}\right)\frac{\eta^3}{6}-4\frac{\eta^2}{2}\right]+(c_5+1)\eta. \tag{41}$$

The examination of the influences of different factors on the distributions of nanoparticles, velocity, and temperature is an important task. By analyzing these effects, we can gain insights into the behavior of the system and understand how different factors influence the properties of the nanoparticles. Once more, we have generated the figures; we can discuss and analyze the observed effects in the following section.

4. Outcomes and debates

In this work, we utilize the HPM method to examine the unsteady Darcy-Forchheimer movement and melting heat transmission of the CNF subjected to the squeezing between two parallel plates, with the incorporation of the influences of slip velocity, thermal radiation, and heat source/sink. Following Eqs. (40) and (41), the numerical results are exhibited graphically through velocity$f'(\eta)$and temperature $\theta(\eta)$distributions for various amounts of the factors, including the squeeze parameter S, heat generation/absorption parameters γ, the porous parameter$K$, the Forchheimer parameter F_r, the magnetic parameter M, the slip parameter a, the melting parameter M_e, the radiation parameter R_d, and the Casson parameter β, as illustrated in Figs. 2–17. We examine the amount of ϕ to indicate both the ground fluid ($\phi = 0$) andFe_3O_4 nanoparticles ($\phi = 0.05$). To this end, the correlations of Eqs. (8)–(11) together with thermo-physical properties of ground liquid and nanoparticle are used as shown in Table 1.[39,45]

This work is conducted for ($S < 0$), which means that the plates move distantly and ($S > 0$) correspond to the convergent movement of two plates,[46] whereas the black curves represent $\phi = 0.05$ and red curves $\phi = 0$. In this work, the calculations have been carried out by taking $M = 0.5$, $S = 2, K = 0.7, M_e = 4, \mathrm{Pr} = 7, F_r = 2, a = 1, \beta = 10, R_d = 0.3$, and$\gamma = 5$. One can see from Figs. 2–17 that Fe_3O_4 nanoparticles reduce the velocity and temperature under the influence of all factors.

- **Velocity distribution**

Figs. 2–11 display the impact of different factors on the velocity of Fe_3O_4 nanofluid. In Fig. 2, the influence of ϕon velocity distribution is reproduced, and it can be apparent that the fraction volume of the nanoparticles plays a role in the performance of the fluid's velocity, that

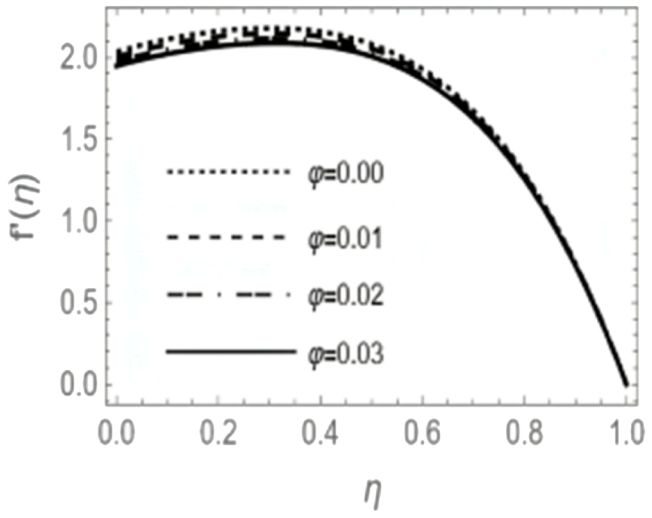

Fig. 2. Velocity distributions for various amounts ofϕ.

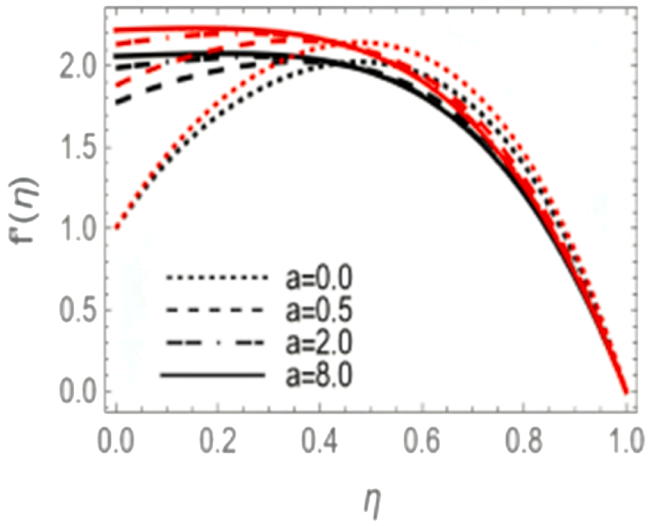

Fig. 3. Velocity distributions for various amounts of a for both ϕ = 0and ϕ = 0.05.

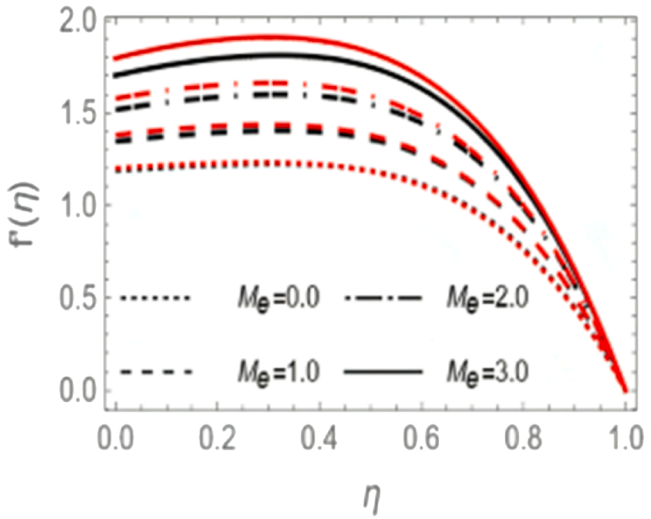

Fig. 4. Velocity distributions for various amounts of M_e for both ϕ = 0and ϕ = 0.05.

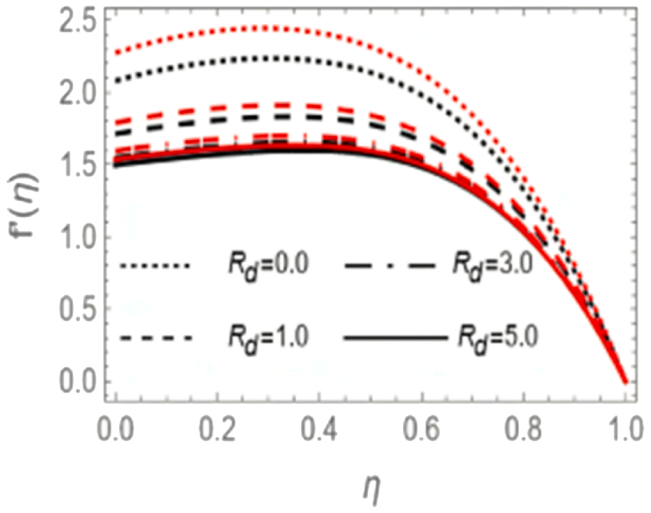

Fig. 5. Velocity distributions for various amounts of $R_d$for both ϕ = 0and ϕ = 0.05.

is, the increase in nanoparticles volume fraction ϕ reduces velocity due to suppression of movement.[26] The variations of $f'(\eta)$ with the slip parameter a are depicted in Fig. 3 for both ground fluid and Fe_3O_4 nanofluid. It is obvious from this figure that there is a growth in the velocity distribution with the augmentation of the slip parameter. From a physical standpoint, the rise in slip velocity is associated with reduced viscous drag or friction at the surface, allowing the fluid to move more freely. Analogous results were previously renowned.[48]

Fig. 4 illustrates the impact of the melting parameter M_e on velocity distribution. It is observed that the growth in the melting parameter results in a growth in velocity for both the base fluid and nanofluid. Physically, the occurrence is a result of the cold sheet when being immersed in warm water, leading to its gradual melting. As the melting continues, the surface gradually transitions to the desired state, causing an increase in velocity and a subsequent decrease in temperature. The scientific explanation for this behavior might involve higher values of a certain factor, which enhances the melting process and behaves similarly to a blowing condition at the surface. Similar outcomes were previously observed.[49]

The variation of velocity under the impact of the radiation parameterR_d is exhibited in Fig. 5; it is observed that the growth in the radiation parameter lessens the velocity for both the ground fluid and the nanofluid. The underlying mechanism of this observation could be that the increased radiation parameter enhances the efficiency of heat dissipation through radiative processes, affecting the fluid's thermal energy and, consequently, its velocity.[49] Fig. 6 represents the impacts of the squeeze parameter S on non-dimensional velocity; we have found that positive and negative values of the squeeze parameter have various impacts on the velocity distribution. The velocity improves as the absolute value of the squeeze parameter grows when two plates move at a distant apart ($S < 0$), meanwhile it decreases as the squeeze number increases in case the two plates move toward together ($S > 0$). These results can be scientifically interpreted that an increase in the squeeze parameter ($S > 0$) might lead to a decrease in velocity due to the narrowing of the movement thickness. Analogous results were previously noted.[45]

Fig. 7 illustrates the impact of the magnetic parameter$M$ on non-dimensional velocity$f'(\eta)$. It is observed that the velocity decreases under the effect of the growth in$M$. When the MF is normal to the

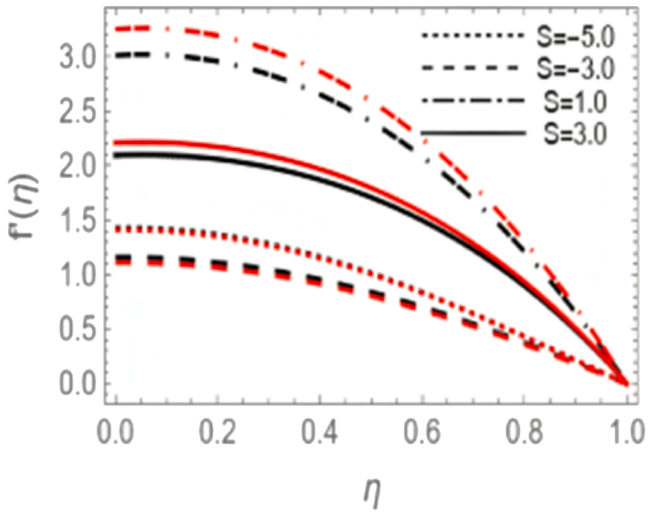

Fig. 6. Velocity distributions for various amounts of S for both $\phi = 0$and $\phi = 0.05$.

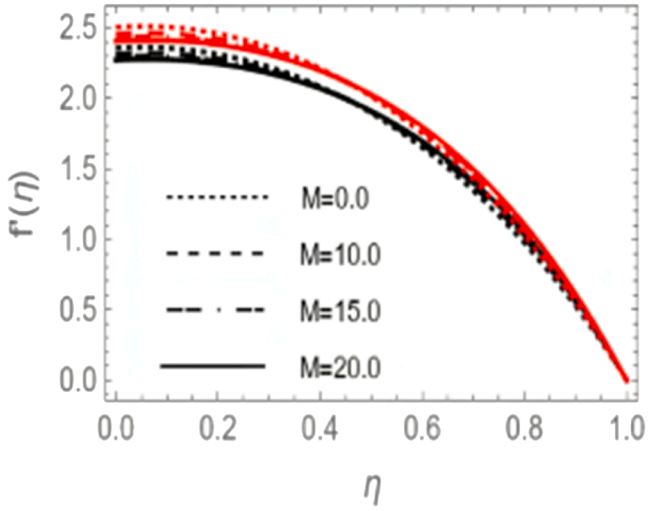

Fig. 7. Velocity distributions for various amounts of M for both $\phi = 0$and $\phi = 0.05$.

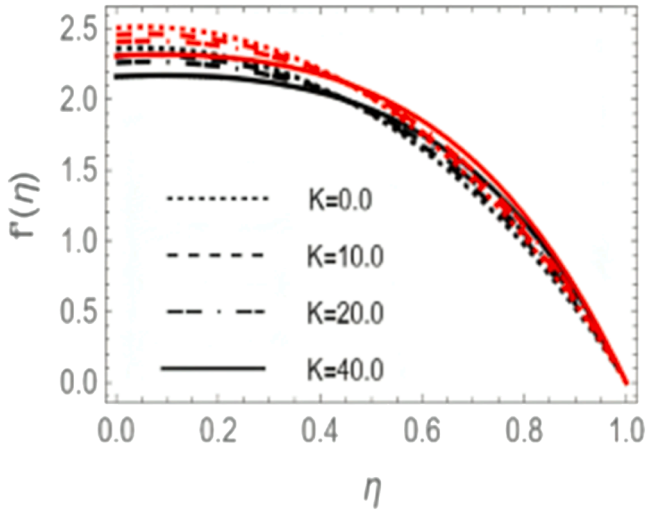

Fig. 8. Velocity distributions for various amounts of K for both $\phi = 0$and $\phi = 0.05$.

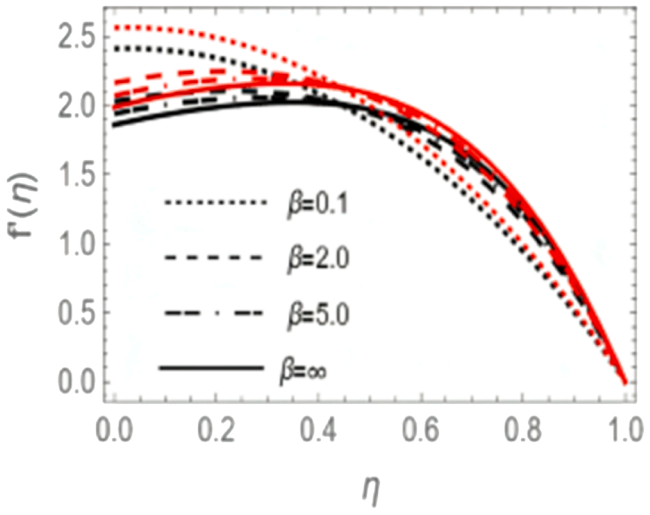

Fig. 9. Velocity distributions for various amounts of β for both $\phi = 0$and $\phi = 0.05$.

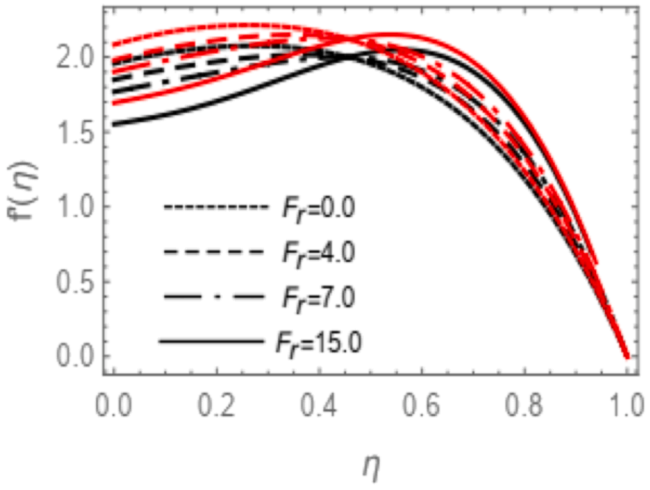

Fig. 10. Velocity distributions for various amounts of F_r for both $\phi = 0$and $\phi = 0.05$.

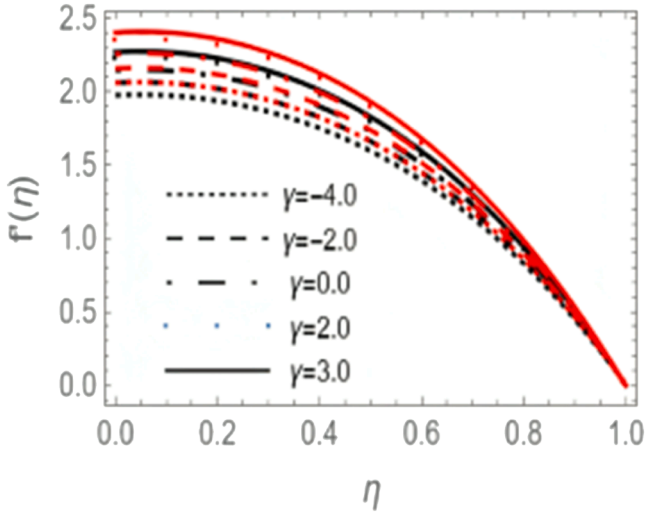

Fig. 11. Velocity distributions for various amounts of γ for both $\phi = 0$and $\phi = 0.05$.

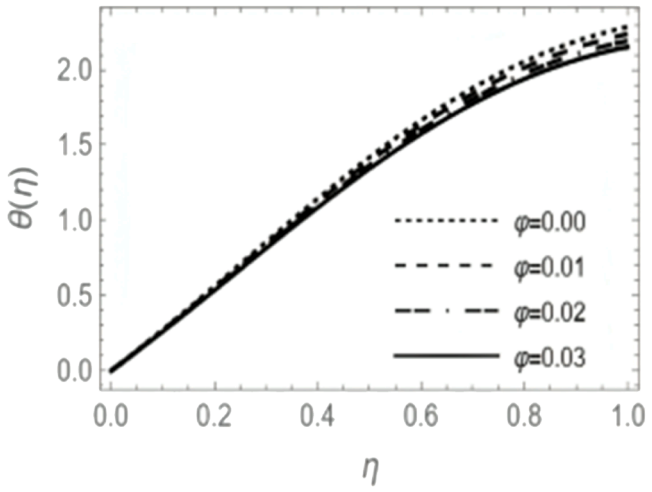

Fig. 12. Temperature distributions for various amounts ofϕ.

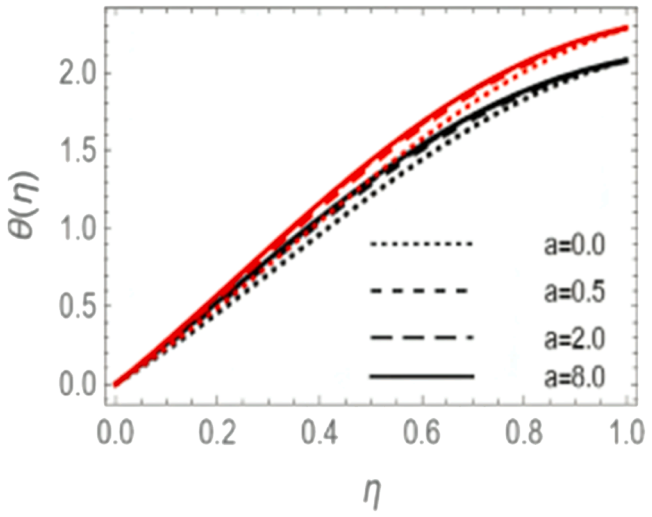

Fig. 13. Temperature distributions for various amounts of a for both $\phi = 0$and $\phi = 0.05$.

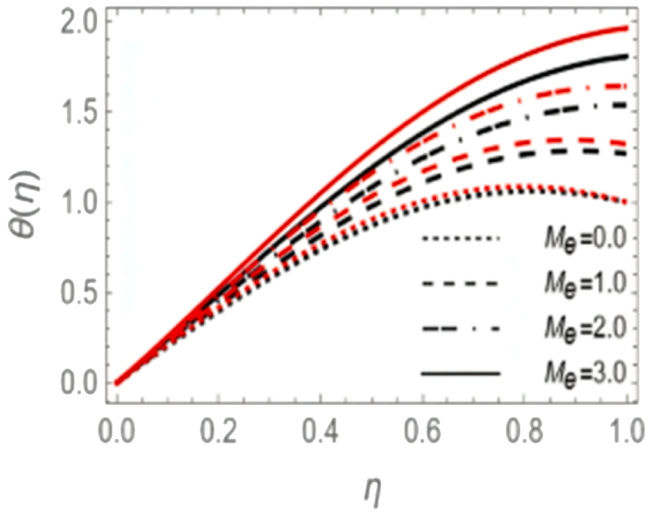

Fig. 14. Temperature distributions for various amounts of M_e for both $\phi = 0$and $\phi = 0.05$.

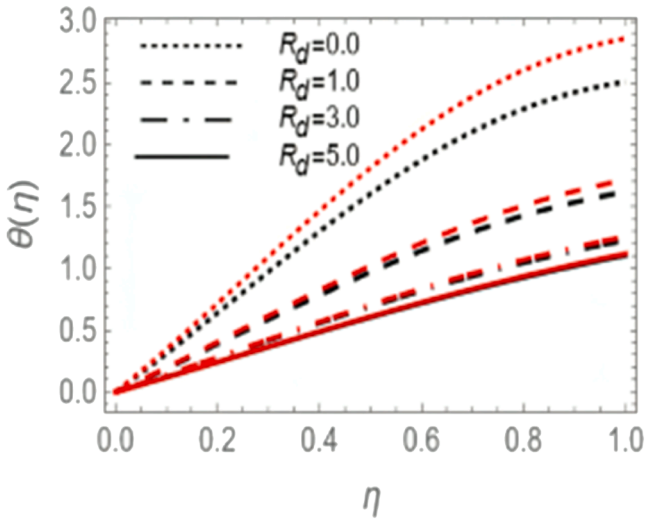

Fig. 15. Temperature distributions for various amounts of R_d for both $\phi = 0$and $\phi = 0.05$.

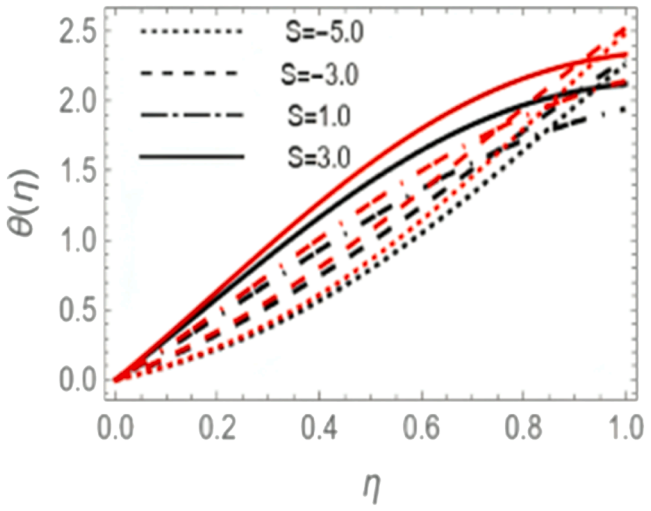

Fig. 16. Temperature distributions for various amounts of S for both $\phi = 0$and $\phi = 0.05$.

direction of movement, this results gives a generation of a resistive drag force called Lorentez force, which results in retiring force to the nano-fluid motion that operates in a direction opposite to the motion, inducing a tendency to decrease the fluid velocity.[50] The change of non-dimensional velocity againstη for various amounts of the porous parameter$K$, is exhibited in Fig. 8. It is found that velocity decreases with the increase in the porous parameter near the lower wall and increases away from it. In fact, the increase in the permeability of the medium resists the movement, which enhances the deceleration of the movement.[51]

The effectiveness of Casson parameterβ on velocity distribution is exhibited in Fig. 9. It is interpreted that the velocity distribution decreases near the lower wall and increases away from it. Indeed, as the Casson parameter β rises, there is a decrease in the yield stress, resulting in a reduction of resistance to the fluid motion, and hence the momentum boundary thickness decreases.[26] Fig. 10 illustrates the variation of velocity under the impact of Forchheimer parameterF_r. It is evident from this figure that there is a diminishing in the velocity distribution with the augmentation of the F_r near the low wall. Alternatively, an obvious opposite pattern is evident away from it. The correlation

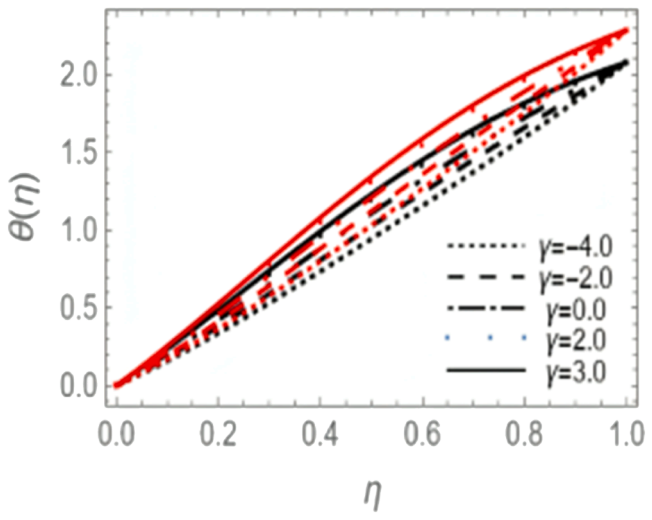

Fig. 17. Temperature distributions for various amounts of γ for both ϕ = 0and ϕ = 0.05.

Table 1
Thermo-physical properties for ground fluid and iron oxide nanoparticles.

Properties	Base Fluid (water)	Fe_3O_4
$c_p(J/kgK)$	4179	670
$\rho(kg/m^3)$	997	5180
$\kappa(W/mK)$	0.613	9.6

between the Forchheimer number and the skin friction coefficient is responsible for the observed pattern in velocity, that is, the constant drag stress generates increased friction transported to the fluid movement, resulting in velocity reduction. Similar outcomes were reported before.[52]

Fig. 11 illustrates the impact of the heat source/sink parameters γ on the velocity distribution, where $\gamma > 0$ identifies the internal heat generation and $\gamma < 0$ identifies the internal heat absorption. It is obvious from Fig. 11 that non-dimensional velocity increases by the increasing of the heat generation, whereas velocity is realized when$\gamma < 0$.

- **Temperature distribution**

The impact of the nanoparticle volumeϕ, the slip parameter a, the melting parameterM_e, the radiation parameter R_d, the squeeze parameter$S$, and heat generation/absorption parameters γ, on the temperature θ(η) for both the base fluid and Fe_3O_4 nanofluid are exhibited in Figs. 12–17. It is observed from Fig. 12 that the reduction in temperature occurs with the increase in nanoparticles volume fractionϕ. So, we can say that the nanoparticle's volume fractionϕ plays an important role in cooling and heating processes.[53] Meanwhile, the increasing slip parameter increases temperature for both the basic fluid and Fe_3O_4 nanofluid as seen in Fig. 13.

Fig. 14 illustrates the impact of the melting parameterM_e on the non-dimensional temperature distribution. It is observed that a growth in the melting parameter results in a growth in temperature for both the base fluid and the nanofluid. This aligns with the physical reality according to which a higher melting parameter indicates a higher rate or extent of solid-to-liquid transition. This phase change often involves the absorption of energy as the solid absorbs heat to undergo melting; this absorption causes a temperature growth.[54]

Figs. 15 and 16 show the impact of the radiation parameter R_d and the squeeze parameter on temperature distribution. From Fig. 15, we can notice that the growth in the radiation parameter diminishes the temperature for both the ground fluid and the nanofluid. The underlying mechanism for this observation could be that the increase in the radiation parameter enhances the efficiency of heat dissipation through radiative processes that affect the fluid's thermal energy. The graph for the temperature θ(η) is plotted for various amounts of the squeeze parameter S in Fig. 16. It is noted that the growth in the magnitude of S is associated with a decrease in the distance between the plates($S > 0$), and the temperature distribution of CNF increases. As the plates separate($S < 0$), the temperature distribution decreases. This performance is due to the fact that the growth in the squeezing parameter represents a growth of friction between plates and nanoparticles, so the temperature of nanofluid increases.

The impishness of the heat generation/absorption parameter γ on the non-dimensional temperature is obvious in Fig. 17 for both the base fluid and Fe_3O_4 nanofluid. It is found that the non-dimensional temperature grows with the rise of the heat generation parameter$\gamma > 0$. However, the growth in the heat absorption parameter$\gamma < 0$ diminishes the non-dimensional temperature, because the energy is emitted at $\gamma > 0$ and this causes an increase in the magnitude of temperature, whereas the energy is realized at$\gamma < 0$, yielding a noteworthy decrease in temperature.[55]

- **Local skin-friction and Nusselt number**

This work is completed by depicting the impact of the dynamic factors on the performance of the local skin-friction and the local Nusselt number. These results are exhibited in Table 2, where the local skin friction and local Nusselt number are derived from definitions as given in Eqs. (20) and (21). From this table, we observe that local skin-friction increases with the rise in the heat generation parameter ($\gamma > 0$), the melting parameterM_e and the absolute value of the squeeze number when two plates move apart ($S < 0$). This is a logical performance because increasing the pressure on the fluid will lead to a growth in its friction with the lower wall and, consequently, an increase in the local skin-friction. On the contrary, we find that the local skin-friction decreases by increasing the volume of nano-particles ϕ, the porous parameter$K$, Forchheimer parameter F_r, the magnetic parameter M, the slip parameter a, the radiation parameter R_d, the heat absorption parameter $\gamma < 0$, the squeeze number ($S > 0$), and Casson parameterβ. In fact, the increase in the Casson parameterβ leads to dominant inertial impacts and then decays the coefficient of skin-friction. However, due to the small size of nan-oparticles and the large surface area, they may act as lubricating agents between the fluid and the solid surface, reducing the frictional forces and, accordingly, the skin friction.[56]

Likewise, we observe various impacts of all factors on local Nusselt number, such as the presence of a negative amount in the wall temperature gradient. The physical interpretation underlying this observation is as follows: the heat is transported from the wall to the surrounding fluid. It is seen that the absolute value of local Nusselt number grows with the rise in the slip parameter a, volume of nanoparticles ϕ, the heat generation parameter $\gamma > 0$, the melting parameterM_e, the squeeze number ($S > 0$). Furthermore, the local Nusselt number decreases with the rise in Casson parameterβ, the heat generation parameter $\gamma < 0$, the radiation parameter R_d and the absolute value of the squeeze number when two plates move apart ($S < 0$). It is seen that other factors have no impact on the Nusselt number; these factors are the porous parameter$K$, Forchheimer parameter F_r, the magnetic parameter$M$.

5. Conclusion

The objective of the study is to examine the dynamics of the MHD flow, considering its unsteady nature, as well as the influence of the Darcy-Forchheimer effect and MHT. The system utilizes a CNF to facilitate heat transmission during the melting process. The slip velocity is affected by the presence of a heat source or sink, as well as thermal radiation. The investigation of the current topic is motivated by the practical applications of squeezing flow in physics. The mathematical

Table 2
Amount of $Cf_x\sqrt{(1-\alpha t)}\mathrm{Re}_x/2$ and $Nu_x\sqrt{(1-\alpha t)}$ for various amounts of $a, \beta, \phi, F_r, \gamma, K, M, M_e, \mathrm{Pr}, R_d$and S.

a	β	ϕ	F_r	γ	K	M	M_e	R_d	S	$Cf_x\sqrt{(1-\alpha t)}\mathrm{Re}_x/2$	$Nu_x\sqrt{(1-\alpha t)}$
0.5	10	0.05	2	5	0.7	0.5	4	0.3	2	1.45107	− 2.663435
1										0.84821	− 2.72218
2										0.46305	− 2.76055
8										0.12429	− 2.79488
	0.1									1.32693	− 2.79738
	2									0.96621	− 2.74171
	5									0.88335	− 2.72807
	10									0.84821	− 2.72218
		0								1.03211	− 2.59259
		0.01								0.98530	− 2.61686
		0.03								0.90807	− 2.66797
		0.05								0.84821	− 2.72218
			0							0.898778	− 2.72218
			4							0.79765	− 272218
			7							0.72180	− 2.72218
			10							0.51955	− 2.72218
				-4						0.54775	− 1.61448
				-2						0.61453	− 1.86064
				0						0.68129	− 2.10678
				2						0.74806	− 2.35294
				3						0.78145	− 2.47602
					0					0.86095	− 2.72218
					10					0.67918	− 2.72218
					20					0.49742	− 2.72218
					40					0.13390	− 2.72218
						0				0.85621	− 2.72218
						10				0.69632	− 2.72218
						15				0.61638	− 2.72218
						20				0.53644	− 2.72218
							0			0.17839	− 2.29547
							1			0.32478	− 2.40215
							2			0.48521	− 2.50883
							3			0.65969	-2.61550
								0		1.01568	− 3.33957
								1		0.66901	− 2.06151
								3		0.51634	− 1.49867
								5		0.46811	− 1.32086
									-5	0.56632	− 1.00603
									-3	0.23847	− 1.59680
									1	1.40709	− 2.29624
									3	0.59199	− 3.04769
									5	0.28830	− 3.63845

procedure entails the transformation of the PDEs into nonlinear ones. The nonlinear ODEs are solved using the HPM, taking into account the relevant BCs. By employing a non-dimensional method, numerous physical values are obtained without any units of measurement. The main outcomes of velocity, temperature profiles, local skin-friction, and the local Nusselt number are displayed and examined according to several dimensionless characteristics. The research delves into the impact of various factors on velocity, temperature base fluid ($\phi = 0$) and Fe_3O_4 nanofluid ($\phi = 0.05$), as well as local skin-friction and local Nusselt number. Some of the key outcomes may be summarized as follows:

- The performance of velocity and temperature are similar for both the ground fluid and the Fe_3O_4 nanofluid under the impact of variation of factors. They decrease as the volume of nanoparticles increases.
- The local skin-friction decreases with the increasing volume of Fe_3O_4 nano-particles. We interpret this performance as follows: as the size of Fe_3O_4 nano-particles increases, they may play a role as a lubricant between the fluid and the wall, then the local skin-friction decreases.
- The increase in the squeeze parameter when two plates move together ($S > 0$) decreases velocity and the local skin-friction, meanwhile, it enhances temperature and local Nusselt number.
- The growth of the squeeze parameter when two plates move at a distance apart ($S < 0$) raises velocity and local skin-friction, while temperature and local Nusselt number decrease.

Future work

In a progress works, we aimed to develop the present work to include other types of biological fluids or hybrid nanofluids**.** We may study the impact of various kinds of nanoparticles and base fluids.

Declaration of competing interest

The authors declare that they have no known competing financial interests or personal relationships that could have appeared to influence the work reported in this paper.

Data availability

Data will be made available on request.

References

1. Vajravelu K, Prasad KV, Ng CO, Vaidya H. MHD squeeze flow and heat transfer of a nanofluid between parallel disks with variable fluid properties and transpiration. *Int J Mech Mater Eng.* 2017;12:9.
2. Memon M, Shaikh AA, Siddiqui A, Kumar L. Analytical solution of slow squeeze flow of slightly viscoelastic fluid film between two circular disks using recursive approach. *Math Probl Eng.* 2022;2022:17. Article ID 4043909.
3. Ahmad S, Farooq M, Anjum A, Mir NA. Squeezing flow of convectively heated fluid in porous medium with binary chemical reaction and activation energy. *Adv Mech Eng.* 2019;11(10):1–12.

4. Ullah I, Rahim MT, Khan H, Qayyum M. Analytical analysis of squeezing flow in porous medium with MHD effect. *UPB Sci Bull Ser A Appl Math Phys*. 2016;78(2): 281–292.
5. Noor NAM, Admon MA, Shafie S. Unsteady MHD squeezing flow of Casson fluid over horizontal channel in presence of chemical reaction. *J Adv Res Fluid Mech Therm Sci*. 2022;92(2):49–60.
6. Jasim AM. Analytical approximation of the first grade MHD squeezing fluid flow with slip boundary condition using a new iterative method. *Heat Transf*. 2020;50: 733–754.
7. Fusi L, Ballotti A. Squeeze low of stress power law fluids. *Fluids*. 2021;6(6):194.
8. Akolade MT, Adeosun AT, Olabode JO. Influence of thermophysical features on MHD squeezed flow of dissipative Casson fluid with chemical and radiative effects. *J Appl Comput Mech*. 2021;7(4):1999–2009.
9. Sobamowo MG, Yinusa AA, Aladenusi ST. Impacts of magnetic field and thermal radiation on squeezing flow and heat transfer of third grade nanofluid between two disks embedded in a porous medium. *Heliyon*. 2020;6:e03621.
10. Obalalu AM. Heat and mass transfer in an unsteady squeezed Casson fluid flow with novel thermophysical properties: analytical and numerical solution. *Heat Transf*. 2021;50:7988–8011.
11. Gangadhar K, Reddy KS, Wakif A. Wall jet plasma fluid flow problem for hybrid nanofluids with Joule heating. *Int J Ambient Energy*. 2023;44(1):2459–2468.
12. Gangadhar K, Kumari MA, Chamkha AJ. EMHD flow of radiative second-grade nanofluid over a Riga plate due to convective heating: revised Buongiorno's nanofluid model. *Arab J Sci Eng*. 2022;47:8093–8103.
13. Gangadhar K, Kumari MA, Rao MVS, Chamkha AJ. Oldroyd-B nanoliquid flow through a triple stratified medium submerged with gyrotactic bioconvection and nonlinear radiations. *Arab J Sci Eng*. 2022;47:8863–8875.
14. Kotha G, Kolipaula VR, Rao MVS, Penki S, Chamkha AJ. Internal heat generation on bioconvection of an MHD nanofluid flow due to gyrotactic microorganisms. *Eur Phys J Plus*. 2020;135. Article Number 600.
15. Gangadhar K, Lakshmi KB, Kannan T, Chamkha AJ. Bioconvective magnetized oldroyd-B nanofluid flow in the presence of Joule heating with gyrotactic microorganisms. *Waves Random Complex Media*. 2022. https://doi.org/10.1080/17455030.2022.2050441. Published online: 21 March.
16. Gangadhar K, Lakshmi KB, El-Sapa S, Rao MVS, Chamkha AJ. Thermal energy transport of radioactive nanofluid flow submerged with microorganisms with zero mass flux condition. *Random Complex Media*. 2022. https://doi.org/10.1080/17455030.2022.2072536. Published online: 12 May.
17. Gangadhar K, Victoria EM, Chamkha AJ. Hydrothermal features in the swirling flow of radiated grapheme - Fe_3O_4 hybrid nanofluids through a rotating cylinder with exponential space-dependent heat generation. *Random Complex Media*. 2022. https://doi.org/10.1080/17455030.2022.2100004. Published online: 21 July.
18. Gangadhar K, Lavanya MR, Chamkha AJ. Multiple convected conditions in Williamson nanofluidic flow with variable thermal conductivity: revised bioconvection model. *Int J Mod Phys B*. 2024;38(05), 2450069.
19. Moatimid GM, Mohamed MAA, Elagamy Kh. Heat and mass flux through a Reiner–Rivlin nanofluid flow past a spinning stretching disc: cattaneo–Christov model. *Sci Rep*. 2022;12. Article Number: 14468.
20. Ullah I, Khan WA, Jamshed W, et al. Heat generation (absorption) in 3D bioconvection flow of Casson nanofluid via a convective heated stretchable surface. *J Mol Liq*. 2023;392, 123503.
21. Kaneez H, Baqar A, Andleeb I, et al. Thermal analysis of magnetohydrodynamics (MHD) Casson fluid with suspended iron (II, III) oxide-aluminum oxide-titanium dioxide ternary-hybrid nanostructures. *J Magn Magn Mater*. 2023;586, 171223.
22. Sajid T, Pasha AA, Jamshed W, et al. Radiative and porosity effects of trihybrid Casson nanofluids with Bödewadt flow and inconstant heat source by Yamada-Ota and Xue models. *Alex Eng J*. 2023;66:457–473.
23. Li Y, Imtiaz M, Jamshed W, et al. Nonlinear thermal radiation and the slip effect on a 3D bioconvection flow of the Casson nanofluid in a rotating frame via a homotopy analysis mechanism. *Nanotechnol Rev*. 2023;12, 20230161.
24. Wang F, Sajid T, Katbar NM, et al. Computational examination of non-Darcian flow of radiative ternary hybridity Casson nanoliquid through rotary cone. *J Comput Des Eng*. 2023;10:1657–1676.
25. Endalew MF. Modeling and analysis of unsteady Casson fluid stream due to an exponentially accelerating plate with thermal and solutal convective boundary conditions. *J Appl Math*. 2023;2023. VolumeArticle ID 3065357.
26. Vishalakshi AB, Mahabaleshwar US, Ahmadi MH, Sharifpur M. An MHD Casson fluid stream past a porous stretching sheet with threshold Non-Fourier heat flux model. *Alex Eng J*. 2023;69:727–737.
27. Reddy CA, Reddy GS, Goud JS, Amarnath N. Casson fluid with over a nonlinear stretching sheet with stagnation point stream, heat and mass transport. *AIP Conf Proc*. 2023;2492(1), 040060.
28. Oke AS, Mutuku WN, Kimathi M, Animasaun IL. Insight into the dynamics of non-Newtonian Casson fluid over a rotating non-uniform surface subject to Coriolis force. *Nonlinear Eng*. 2020;9:398–411.
29. Abd El-Aziz M, Afify AA. MHD Casson fluid stream over a stretching sheet with entropy generation analysis and Hall influence. *Entropy*. 2019;21(6):592, 20 Pages.
30. Moatimid GM, Mohamed MAA, Elagamy KH. A Casson nanofluid stream within the conical gap between rotating surfaces of a cone and a horizontal disc. *Sci Rep*. 2022; 12:11275.
31. He JH. Homotopy perturbation technique. *Comput Methods Appl Mech Eng*. 1999;178 (3–4):257–262.
32. Vijayalakshmi T, Senthamara R. Application of Homotopy perturbation and variational iteration methods for nonlinear imprecise prey–predator model with stability analysis. *J Supercomput*. 2022;78:2477–2502.
33. Rehman G, Qin S, Ain QT, et al. A study of moisture content in unsaturated porous medium by using Homotopy perturbation method (HPM) and variational iteration method (VIM). *GEM Int J Geomath*. 2022;13:3–13.
34. Qian WM, Riaz A, Ramesh K, et al. Mathematical modeling and analytical examination of peristaltic transport in stream of Rabinowitsch fluid with Darcy's law: two-dimensional curved plane geometry. *Eur Phys J Spec Top*. 2022;231(4): 545–555.
35. Moatimid GM, Zekry MH, Gad NS. Nonlinear EHD instability of a cylindrical interface between two Walters' B fluids in porous media. *J Porous Media*. 2022;25 (3):11–34.
36. Moatimid GM. Sliding bead on a smooth vertical rotated parabola: stability configuration. *Kuwait J Sci*. 2020;47(2):6–21.
37. Moatimid GM. Stability analysis of a parametric Duffing oscillator. *J Eng Mech*. 2020;146(5), 0502000.
38. Moatimid GM, Mohamed MAA, Elagamy KH. A motion of Jeffery nanofluid in porous medium with motile microorganisms between two revolving stretching discs: effect of Hall currents. *J Porous Media*. 2022;25(10):83–101.
39. Khan Z, Ghoneim ME, Zuhra S, Ali A, Tag-Eldin E. Numerical solution of Rosseland's radiative and magnetic field effects for Cu-Kerosene and Cu-water nanofluids of Darcy-Forchheimer stream through squeezing motion. *Alex Eng J*. 2023;64(1): 191–204.
40. Hayat T, Nassem AU, Khan MI, Farooq M, Alsaedi A. Magnetohydrodynamic (MHD) stream of nanofluid with double stratification and slip conditions. *Phys Chem Liq Intern J*. 2017;7:1–20.
41. Megahed AM. Effect of slip velocity on Casson thin film stream and heat transport due to unsteady stretching sheet in presence of variable heat flux and viscous dissipation. *Appl Math Mech*. 2015;36(10):1273–1284.
42. Salehi S, Nori A, Hosseinzadeh KH, Ganji DD. Hydrothermal analysis of MHD squeezing mixture fluid suspended by hybrid nanoparticles between two parallel plates. *Case Stud Therm Eng*. 2020;21, 100650.
43. Imtiaz M, Shahid F, Hayat T, Alsaedi A. Melting heat transport in Cu-water and Ag-water nanofluids stream with homogeneous-heterogeneous reactions. *Appl Math Mech*. 2019;40(4):465–480 (English Edition).
44. Madaki AG, Roslan R, Mohamad M, Kamardan MG. Analytical solution of squeezing unsteady nanofluid stream in the presence of thermal radiation. *J Comput Sci Comput Math*. 2016;6(4):97–103.
45. Brewster MQ. *Thermal Radiative Transport Properties*. New York: John Wiley &Sons; 1992.
46. Noor NAM, Shafie S. Magnetohydrodynamics squeeze stream of sodium alginate-based Jeffrey hybrid nanofluid with heat sink or source. *Case Stud Therm Eng*. 2023; 49, 103303.
47. Zangooee MR, Hosseinzadeh KH, Ganji DD. Hydrothermal analysis of hybrid nanofluid stream on a vertical plate by considering slip condition. *Theor Appl Mech Lett*. 2022;12(5), 100357.
48. Abdel-Rahman RG, Khader MM, Megahed AM. Melting phenomenon in magneto hydro-dynamics steady stream and heat transport over a moving surface in the presence of thermal radiation. *Chin Phys B*. 2013;22(3), 030202.
49. Elfeshawey AS, Waheed SE. Effect of viscous dissipation and thermal radiation on MHD stream and heat transport for a power law fluid with variable fluid properties over a permeable stretching sheet. *Waves Random Complex Media*. 2022. https://doi.org/10.1080/17455030.2022.2053610.
50. Muhammad K, Abdelmohsen SAM, Abdelbacki AMM, Ahmed B. Darcy-Forchheimer stream of hybrid nanofluid subject to melting heat: a comparative numerical study via shooting method. *Int Commun Heat Mass Transp*. 2022;135, 106160.
51. Memon MA, Sagheer DS, Al-Malki MAS, et al. Squeezed Darcy–Forchheimer Casson nanofluid stream between horizontal plates under the effect of inclined magnetic field. *Nanoscale Adv*. 2023;5:6925–6934.
52. Freidoonimehr N, Rashidi MM, Mahmud S. Unsteady MHD free convective stream past a permeable stretchingvertical surface in a nano-fluid. *Int J Therm Sci*. 2015;87: 136–145.
53. Hayat T, Muhammad T, Qayyum A, Alsaedi A, Mustafa M. On squeezing stream of nanofluid in the presence of magnetic field effects. *J Mol Liq*. 2016;213:179–185.
54. Dinarvand S, Berrehal H, Tamim H, Sowmya G, Noeiaghdam S, Abdollahzadeh M. Squeezing stream of aqueous CNTs-Fe_3O_4 hybrid nanofluid through mass-based approach: effect of heat source/sink, nanoparticle shape, and an oblique magnetic field. *Results Eng*. 2023;17, 100976.
55. Khan U, Khan SI, Ahmed N, Bano S, Mohyud-Din ST. Heat transport analysis for squeezing stream of a Casson fluid between parallel plates. *Ain Shams Eng J*. 2016;7: 497–504.